Synthesis and characterization of mixed sodium and lithium fullerides for hydrogen storage

Mattia Gaboardi, Nicola Sarzi Amadè, Mauro Riccò, Chiara Milanese, Alessandro Girella, Marta Gioventù and Felix Fernandez-Alonso

Published version information

Citation: M Gaboardi et al. "Synthesis and characterization of mixed sodium and lithium fullerides for hydrogen storage." International Journal of Hydrogen Energy, vol. 43, no. 34 (2018): 16766-16773.

DOI: 10.1016/j.ijhydene.2018.03.210

Synthesis and characterization of mixed sodium and lithium fullerides for hydrogen storage

Mattia Gaboardi,*[a] Nicola Sarzi Amadè,[b] Mauro Riccò,[b] Chiara Milanese,[c] Alessandro Girella,[c] Marta Gioventù,[c] and Felix Fernandez-Alonso.[a,d]

[a] *ISIS Facility, Rutherford Appleton Laboratory, Harwell Campus, Chilton, Didcot, United Kingdom*

[b] *Dipartimento di Scienze Matematiche, Fisiche e Informatiche, Universitá di Parma, Viale delle Scienze, 7/a, 43124 Parma, Italy.*

[c] *C.S.G.I. & Dipartimento di Chimica, Sezione di Chimica Fisica, Universitá degli Studi di Pavia, Viale Taramelli 16, 27100 Pavia, Italy.*

[d] *Department of Physics and Astronomy, University College London, Gower Street, London, WC1E 6BT, UK.*

We herein report on the synthesis of mixed alkali cluster intercalated fullerides $Na_xLi_{y-x}C_{60}$ (y=12; x=1-6) by a two-steps mechanochemical reaction of fullerene with sodium and lithium. These compounds crystallize in the cubic lattice of C_{60} displaying a contracted lattice parameter with respect to the Na_6C_{60} parent structure. The analysis of the hydrogen sorption behaviour shows a slight decrease in the dehydrogenation enthalpy for y=12 with respect to the sodium free member. Raman spectroscopy highlighted a partial electron transfer from alkali metals to C_{60}, suggesting the presence of charged sodium/lithium clusters. Finally, we applied muon spectroscopy to understand the different hydrogenation mechanisms in $Na_xLi_{6-x}C_{60}$ and $Na_xLi_{12-x}C_{60}$ and explain their different performance.

I. INTRODUCTION

Intercalated fullerides have gained renewed interest in the field of energy storage for their performance as hydrogen-absorbing materials[1–5]. Sodium (Na) or lithium (Li) doping of Buckminster fullerene C_{60} in a molar ratio greater than four (*i.e.* A_xC_{60}, x>4. A=Na, Li) results in a face-centred-cubic (*fcc*) arrangement of C_{60} molecules with alkali ions occupying the large interstitial sites of the fullerite structure. For each fullerene, the *fcc* lattice hosts two tetrahedral (TH) sites and an octahedral one (OH), virtually allowing a maximum doping of x=3. However, the OH site is large enough to host a small alkali cluster. Examples include $Na_{10}C_{60}$ and $Li_{12}C_{60}$[6,7], where a *bcc* and an *fcc* cluster of Na/Li are formed respectively. For such high doping levels, the number of alkali ions exceeds the maximum amount of electrons that can virtually populate the lowest degenerate unoccupied molecular orbital (LUMO) on fullerene, the latter being able to host six electrons, but the metal clustering can overcome this instability. $Na_{10}C_{60}$ and $Li_{12}C_{60}$ can reversibly absorb up to 3.0 and 5.2 wt% H_2 with a relative dehydrogenation enthalpy of about 66 and 52 kJ/mol H_2, respectively[8,9]. The absorption process leads to a partial segregation of NaH or LiH, achieved after hydrogenation of the fullerene molecule.

$$M_xC_{60} + \frac{y}{2}H_2 \rightleftharpoons M_{x-z}C_{60}H_{y-z} + zMH, \qquad (1)$$

where M=Na, Li. Overall, the Na intercalated compounds show lower absorption capacity with improved kinetics, working temperature, and desorption enthalpies[8]. On the other hand, Li has the advantage to be lighter than Na and higher levels of absorption can be achieved when it is intercalated. Recently, we managed to find an optimal sorption performance by synthesizing mixed Na and Li doped fullerides with composition $Na_xLi_{6-x}C_{60}$. These phases have demonstrated better performance with respect to Li_6C_{60} for x<2, reaching a full absorption at 553 K and 100 bar H_2, with 44 kJ/mol H_2 desorption enthalpy[10]. With this paper, we extend the study of the Na-Li mixed phases for the high-stoichiometric compounds $Na_xLi_{12-x}C_{60}$, hereby reporting on the synthesis, structure, Raman spectroscopy, hydrogen sorption analysis, and muon spectroscopy of these novel fullerides.

II. MATERIALS AND METHODS

All the synthetic procedures and handling of materials were carried out by operating under vacuum or inside He or Ar filled glove boxes (O_2 and H_2O levels <1 ppm). $Na_xLi_{12-x}C_{60}$ samples were synthesized in a two-steps procedure through high-energy ball milling (Fritsch Mini-Mill P23; ZrO_2 bowl with 5 balls). In the first step, C_{60} powder (M.E.R., 99+%) and the relative molar ratio of Na (Alfa Aesar, 99.95%) were milled at 30 Hz for 1 hour (3 times 20 min each, separated by a 5 min break). The so-obtained black powder is subsequently milled under the same conditions with a stoichiometric amount of Li (Sigma-Aldrich, 99% granular), previously cut in small flakes. Each sample was then pelletized under 1.5 tons (9 mm diameter pellets, about 150 mg each), placed in stainless-steel cylinders closed with a screw cap, and sealed in borosilicate vials under high vacuum ($p<10^{-5}$ mbar). Thermal annealing was carried out in static vacuum at 673 K for 5 days. $Na_xLi_{6-x}C_{60}$ samples were synthesized as previously reported[10]. X-ray powder diffraction (XRPD) was carried out on 0.7 mm diameter and 0.01 mm wall-thickness capillaries using a Xenocs Nano-inXider diffractometer, operating in wide-angle X-ray scattering mode (WAXS). Raman spectroscopy was

carried out at room temperature by means of a Bruker Senterra Raman microscope operating with 20x or 50x objective. Powders in the capillaries were analysed using 785 nm and 532 nm laser wavelengths at relatively low power density(<200 W/cm^2) and short acquisition time to avoid radiation damage on the specimen. Hydrogen absorption investigations were performed on the as-prepared samples in a PCTPro-2000 manometric instrument (Hy-Energy & Setaram). About 300 mg of each sample was heated from room temperature up to 553 K at 5 K/min under 100 bar H_2 and a 10 h isothermal step was appended at the end of the ramp. H_2-desorption kinetic measurements were performed by heating the samples at 673 K under 0.5 bar of hydrogen and appending 10 h of isotherm. Four sorption cycles were performed for each sample to verify the cycling ability of the samples. Coupled calorimetric-manometric measurements were performed by connecting the high-pressure stainless-steel cell of a Sensys high-pressure DSC (Setaram) with the PCTPro equipment. About 30 mg of the samples hydrogenated in the first charging run were dehydrogenated by heating from room temperature up to 673 K at 0.5 bar of H_2 in dynamic mode (heating rate of 5 K/min). The uncertainty for the H_2 ab/de-sorption wt% values and for the desorption enthalpies are in the order of ±0.3 wt% and ±2 kJ/mol H_2 respectively. Muon spin relaxation (μSR) experiments were carried out at the ISIS Facility, RAL (Didcot, UK), on the EMU spectrometer. The 100% spin-polarized pulsed beam of this facility is optimized to study the muon-spin evolution over long time-scales. The total experimental muon polarization asymmetry was estimated on a separate transverse field (TF) experiment on pure silver. The baseline, due to muons stopping outside the sample, was measured to be 3% of the total polarization at zero field (ZF), whereas its longitudinal field (LF) dependence was measured applying a field in the range 0 - 3.8 kG and was considered in order to extract the repolarization data. For each sample, about 300 - 400 mg of powder was pressed and sealed in an air-tight silver-coated aluminium cell, capped by a kapton window. The muon polarization is followed by plotting the asymmetry function, expressed as $A(t)=(N_b(t)-\alpha N_f(t))/(N_b(t)+\alpha N_f(t))$, where $N_{(b,f)}$ is the backward/forward collected counts and α is a geometrical parameter, calibrated for each temperature by fitting the oscillation observed under the application of a 20 G transverse field. The time-dependent polarization was analysed by means of the WiMDA software[11].

III. RESULTS

Diffraction. XRPD patterns for $Na_xLi_{12-x}C_{60}$ samples for x=0, 1, 2, 3, and 6 are reported in Fig. 1. Synthesized samples appear as single phases characterized by an apparent high symmetry. Diffraction patterns showed broad lines, ascribed to disorder in the fulleride structure. Data were analysed by means of Le Bail pattern decomposition using the *fcc* cell of C_{60}. Similar to the parent low-stoichiometric compounds $Na_xLi_{6-x}C_{60}$, we expect a disordered occupation of Na and Li sites, as well as the presence of rotational disorder for C_{60} molecules[10,12]. The emergence of the 400 peak intensity at around 25.4° with the increase of x suggests a higher occupancy of Na in the *4b* ($\frac{1}{2},\frac{1}{2},\frac{1}{2}$) and *8c* ($\frac{1}{4},\frac{1}{4},\frac{1}{4}$) sites, rather than in the *32f* (x,x,x) positions. This observation is also in agreement with the smaller lattice expansion of $Na_6Li_6C_{60}$ (a=14.244(2) Å) as compared to Na_6C_{60} (a=14.380 Å[13]) and $Na_{10}C_{60}$ (a=14.590 Å[6]), where the *32f* sites are occupied by Na forming a tetrahedral (Na_6C_{60}) or *bcc* ($Na_{10}C_{60}$) cluster in the OH interstice. Specific values for the lattice parameters are reported in table SI1. The relatively high contraction of the unit cell is also found in Li_6C_{60} and $Li_{12}C_{60}$, where the strong electrostatic interaction between Li ions and the negatively charged fullerene molecules shrinks the lattice volume[7]. Fig. 2 shows the effect of hydrogen sorption on the $Na_xLi_{12-x}C_{60}$ diffraction patterns. After the first absorption at 553 K (Fig. 2(a)), the *fcc* features of $Li_{12}C_{60}$ are broader and the peaks shifted to lower angles, suggesting the expansion of the cell upon formation of the hydrofullerene molecule[12]. For x=1-6, the diffrac-

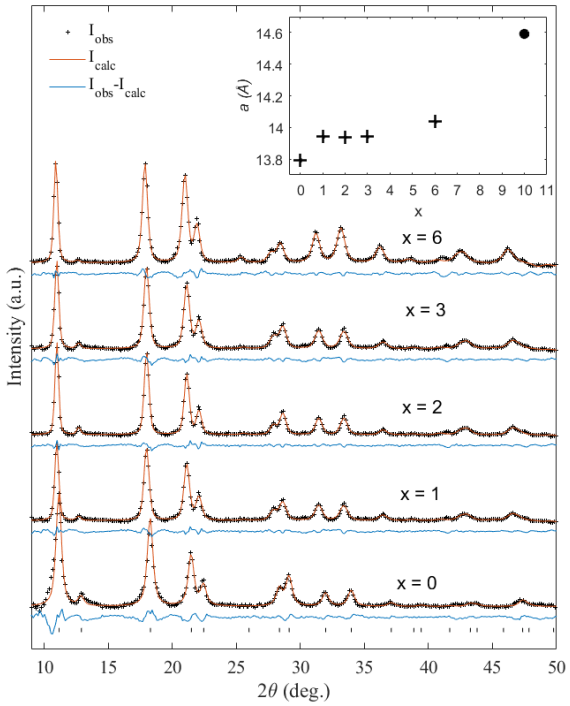

FIG. 1. XRPD patterns for the $Na_xLi_{12-x}C_{60}$ samples and Le-Bail pattern decomposition starting from the *fcc* cell of C_{60} (indexed by tick marks). Backgrounds have been subtracted and data normalized for comparison. Inset: refined cubic lattice parameters of $Na_xLi_{12-x}C_{60}$ (crosses) and the case of $Na_{10}C_{60}$ (dots)[6].

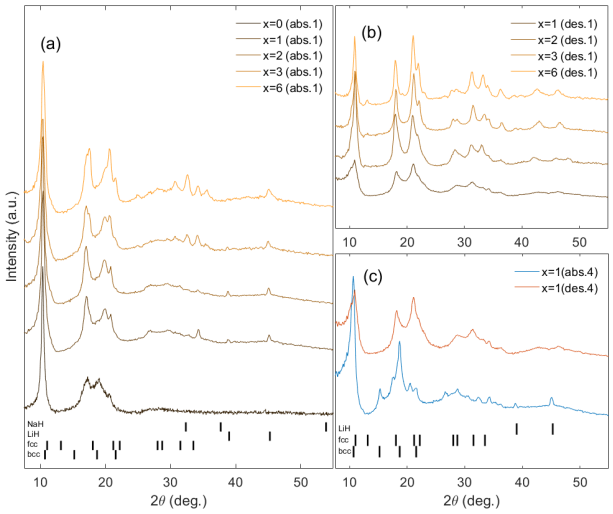

FIG. 2. XRPD patterns of $Na_xLi_{12-x}C_{60}$ as measured after (a): first absorption at 553 K and 100 bar H_2; (b): first desorption at 673 K; and (c): fourth absorption and fourth desorption cycle under the experimental conditions reported above for the x=1 sample.

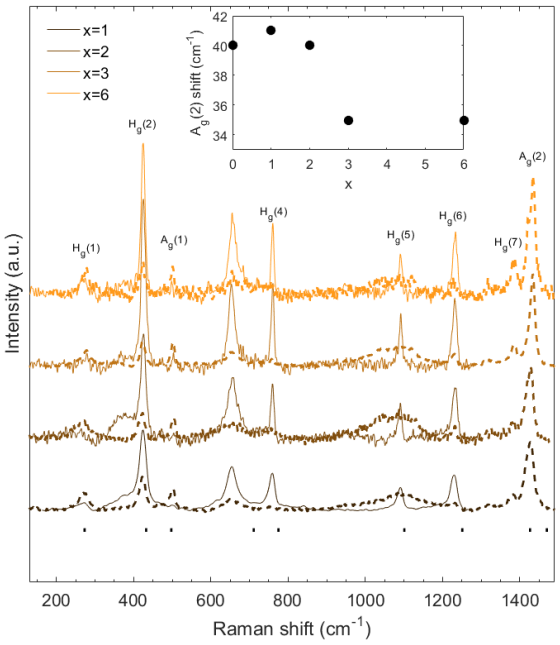

FIG. 3. Raman spectra of $Na_xLi_{12-x}C_{60}$ desorbed at 673 K using an excitation wavelength at λ=785 nm (solid line) and 532 nm (dashed line), after suitable subtraction of the background and normalization. Tick marks represent the Raman active modes of fullerite. Peaks are labelled according to the modes of the C_{60} monomer. Inset: Raman shift of the $A_g(2)$ mode as a function of x.

tion patterns display the peaks of the *fcc* phase of fullerite, although the 220, 311, and 222 *fcc* reflections are probably the convolution of more peaks resulting from a slight lowering of symmetry. A more precise evaluation of the structure would require higher resolution (*i.e.* data from a synchrotron source). The hydrogenation also involves the formation of LiH as secondary phase, whereas NaH was not detected up to x=6. After the first desorption at 673 K we observe the restoration of *fcc* symmetry (Fig. 2(b)). After the fourth sorption cycle (*e.g.* see Fig. 2c for x=1), the samples hydrogenated at 553 K show the coexistence of both *fcc* and *bcc* phases and LiH, while the desorbed sample reproduces the *fcc* reflections, suggesting full reversibility of the process, at least up to four cycles.

Raman Spectroscopy. The as-synthesized compounds are characterized by a very high absorption of visible light and the spectroscopy of these samples was not possible. Fig. 3 shows the Raman spectra of $Na_xLi_{12-x}C_{60}$ after the first desorption at 673 K. We used two different wavelengths in order to maximize the information, due to the different Raman scattering of fullerides to green (532 nm) and near-infrared (785 nm) light. In particular, with λ=785 nm is possible to overcome the problem of sample fluorescence, although the high-frequency peaks (*i.e.* above 1300 cm^{-1}) appear too weak and broad to be resolved. On the other hand, the 532 nm laser is better suited to study the high frequency region. By combining the two wavelengths it was possible to detect most of the first-order A_g and H_g Raman-active modes expected form the fullerene molecule. Most of the peaks shift to red after the intercalation by Na and Li. The shift of the $A_g(2)$ "pentagonal pinch" mode, associated with the charge transfer on C_{60} through the empirical rule of 6.1 cm^{-1} downshift per electron transferred[14], is of particular interest. After the first dehydrogenation, the $A_g(2)$ peak is downshifted to 1428 cm^{-1} for x=1 (with respect to 1469 cm^{-1} of C_{60}), corresponding to about 6.7 electrons. The shift is slightly lower with increasing Na content (see inset). For x>2 the $A_g(2)$ peak is located at 1435 cm^{-1}, corresponding to 5.6 electrons. For all compositions the $A_g(1)$ mode is upshifted from 270 cm^{-1} to about 502 cm^{-1}. It is worthwhile noticing that the peak at about 655 cm^{-1} does not correspond to any Raman-active mode for icosahedral symmetry and seems to be barely affected by variations in the Na stoichiometry. A shift of 54 cm^{-1} for the $H_g(3)$ mode from the 709 cm^{-1} value of C_{60} appears to be unlikely. The activation of this mode can either be ascribed to the presence of disorder or lowering of the icosahedral symmetry of C_{60}. Upon polymerization, we should observe the activation of a plethora of modes in the region 400 - 750 cm^{-1}, corresponding to the (usually silent) modes that are activated after the formation of C-C single or double bonds occurring between neighbouring C_{60} monomers[15]. However, the XRPD analysis does not suggest the occurrence of polymerization. The unassigned peak is lo-

cated in the region of the 5-fold degenerate IR active $H_u(3)$ mode. We tentatively ascribe the activation of this mode to the symmetry-breaking from icosahedral geometry of fullerene as a result of the partial hybridization of C_{60} and Li (or cluster) orbitals or to the preferential anisotropic orientation of molecules that break the cubic and inversion symmetry.

H_2 sorption. The H_2 sorption study on the $Na_xLi_{6-x}C_{60}$ family has been recently reported[10]. In these compounds (*i.e.* for y=6) a low amount of intercalated Na (x=0.5, 1) was found to improve both the hydrogenation and dehydrogenation temperature and kinetics, also lowering the dehydrogenation enthalpy. An optimal condition was found for x=1, for which 4.4 wt% H_2 is stored at 553 K and 100 bar H_2 with an absorption rate of $7{\cdot}10^{-2}$ wt%min^{-1} H_2 and further desorbed at 556 K (1 bar H_2) with ΔH_{des}=44 kJ/mol H_2. For comparison, we underline that Li_6C_{60} can desorb about 5 wt% H_2 with an enthalpy of 61 kJ/mol H_2 and a peak temperature of 579 K after absorption of the same H_2 amount at 623 K and 100 bar H_2 with a rate of $3.9{\cdot}10^{-2}$ wt%min^{-1}. Fig. 4 displays the H_2 absorption kinetics at 553 K and 100 bar H_2 (a) and the desorption up to 673 K (b) of the $Na_xLi_{12-x}C_{60}$ samples (*i.e.* y=12). The characteristic values for the different samples are reported in Table I. The trend obtained for the $Na_xLi_{12-x}C_{60}$ family is a

TABLE I. characteristic kinetic and thermodynamic data for the $Na_xLi_{12-x}C_{60}$ samples.

x	wt.%	v(wt%/min)	T^{on}_{des}(K)	ΔH_{des}(kJ/mol H_2)
0	4.9	$5.7{\cdot}10^{-2}$	548	60.5
1	4.4	$5.5{\cdot}10^{-2}$	556	59.2
2	4.6	$5.9{\cdot}10^{-2}$	559	59.9
3	3.7	$5.6{\cdot}10^{-2}$	547	54.1
6	2.8	$3.1{\cdot}10^{-2}$	546	47.8

decrease in the H_2 capacity but also in the desorption enthalpy (ΔH_{des}) and in the desorption onset temperature (T^{on}_{des}) by increasing the Na amount, testifying the role of the metal in the destabilization of the hydrogenated fulleride compounds. The absorption rate (v_{abs}) is quite similar for all the compounds apart from the one richest in Na, that shows a drop in this value. In general, the absorption kinetics of these samples are slower than the ones measured for the $Na_xLi_{6-x}C_{60}$ compounds[10]. The reversibility of the samples is good, since the performance reported in Table I are maintained also after 4 sorption cycles.

Hydrogenation mechanisms. Muon spectroscopy is a useful tool to study the formation of hydrogenated species in materials and can provide unique insights on both the sorption mechanisms and ion dynamics. Positive muons are spin-$\frac{1}{2}$ particles sharing the same charge of protons. In a muon spin relaxation (μSR) experiment,

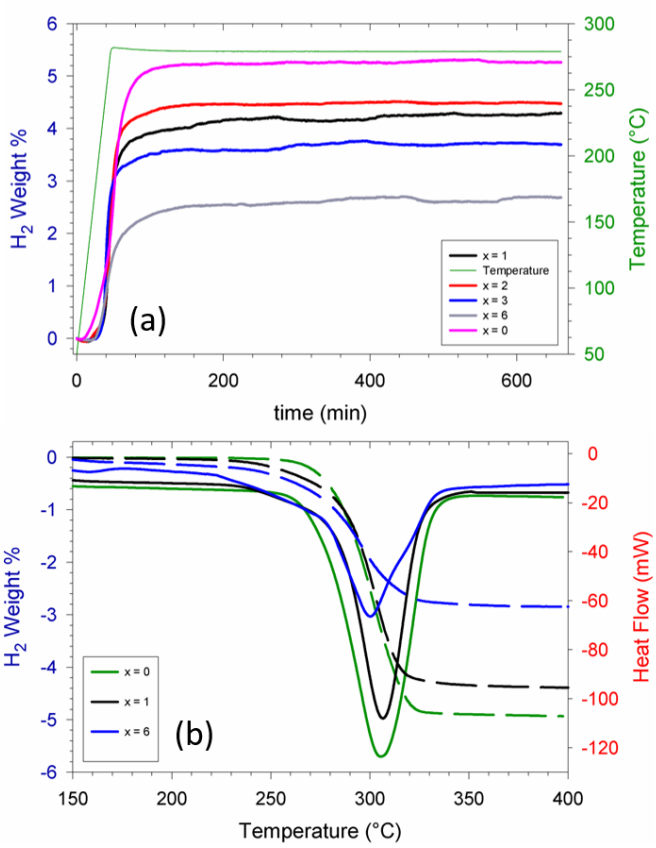

FIG. 4. Hydrogen sorption kinetics for the $Na_xLi_{12-x}C_{60}$ samples. (a) Absorption manometric curves. (b) Coupled manometric−calorimetric desorption curves (shown for selected samples).

100% spin-polarized muons (μ^+) are implanted in the specimen, acting as local magnetic probes[16]. Muon thermalization in non-metallic materials often leads to the formation of muonium (Mu), a light isotope of hydrogen. As observed in previous studies[17], in light fullerides, muonium can form endohedral muonium (*i.e.* a Mu trapped inside the C_{60} cage, or Mu@C_{60}) or it can further react with an unsaturated double-bond on fullerene, forming a radical adduct (Mu-C_{60})[18]. Alkali-cluster-intercalated fullerides have been recently investigated by means of μSR and showed peculiar behaviour. In Li_6C_{60} and $Na_{10}C_{60}$, a large fraction of muons form a stable Mu-C_{60} radical[19], whose hyperfine frequency increases linearly with the degree of C_{60} hydrogenation[19,20]. Conversely, in $Li_{12}C_{60}$, Mu reacts with Li clusters forming a stable Li-Mu species characterized by a covalent bond (d $\sim$ 1.62 Å).

$Na_xLi_{12-x}C_{60}$ compounds (y=12) Fig. 5 shows the μSR results obtained in the case of $Na_xLi_{12-x}C_{60}$. For each sample, about 25% of the expected total asymmetry is missing. This is generally a fingerprint of the formation of paramagnetic species (*i.e.* muonium). When muonium is formed, the hyperfine interaction between the muon

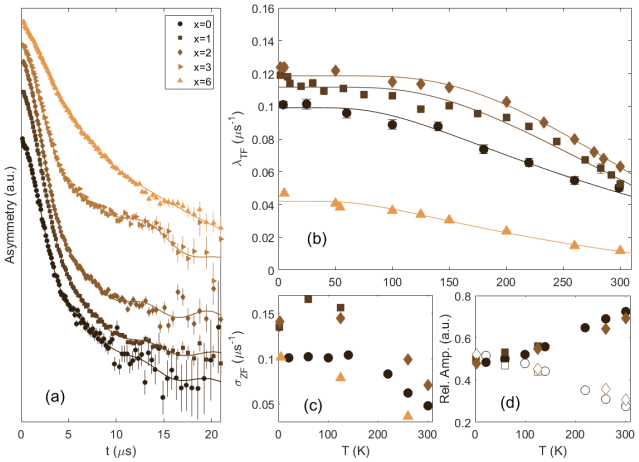

FIG. 5. (a) ZF μSR of $Na_xLi_{12-x}C_{60}$ (x=0-3 and 6) at 5 K and fit (solid lines) as described in the text. Asymmetries are shifted and rebinned for clarity. (b) Lorentzian relaxation rates in transverse field (for x=0-2 and 6) and fit to an activated law (solid lines). (c) ZF decay of the relaxing component: Gaussian for x=0-3 and Lorentzian for x=6. (d) Relative amplitudes (x=0-2) of the Mu-Li (void dots) and μ^+ components (white dots).

and the electron spins gives rise to a high muon precession frequency that exceeds the instrumental cut off (about 10 MHz). This fast oscillation is averaged to zero, resulting in a missing fraction. A further investigation in longitudinal field (see Fig. SI1 in Supporting Information) highlighted the formation of endohedral muonium for x=1. The formation of muon radical adducts is very likely to occur, as observed by the non-flat repolarization below 1 kG. However, their identification is complicated by the very low fraction (below 10% of the missing asymmetry). For x=1-3 the ZF data were fitted according to the function previously reported for $Li_{12}C_{60}$[21], which consists of the sum of a slow-oscillating component and a Gaussian:

$$P_\mu(t) = A_1 P_1(\nu_d, \nu_Q, t)\exp(-\lambda_1 t) + (1-A_1)\exp(-\sigma_{ZF}^2 t^2) \quad (2)$$

Here, P_1 is a function describing the heteronuclear dipolar coupling with ^{7}Li nuclear spins (I=$\frac{3}{2}$), ν_d and ν_Q are the dipolar and quadrupolar frequencies respectively[22,23], and λ_1 is the associated decay rate. σ_{ZF} represents the decay rate of the Gaussian component associated with the spins of the diamagnetic muons (μ^+) interacting with ^{7}Li and ^{23}Na (I=$\frac{3}{2}$) nuclear magnetic moments (the small natural abundance of ^{13}C and ^{6}Li gives a negligible contribution). For x=6, a simple Lorentzian decay reproduces the data well. A small longitudinal field of about 50 G is enough to flatten all the ZF decays, confirming the dipolar nature of the relaxations. For each specimen, at 5 K ZF data were fitted according to Eq.2 and the values found for ν_d, ν_Q, and λ_1 were kept constant for all the other temperatures, while fitting only σ_{ZF} [Fig. 5(c)] and A_1 [Fig. 5(d)]. An average value of ν_d=30.3(4) kHz and ν_Q=38.1(6) kHz was obtained for x=1-3, very close to what found for $Li_{12}C_{60}$ [35(2) kHz and 41(3) kHz respectively][21]. Such values correspond to an average Mu-Li distance of about 1.7 Å, close to a covalent bond[24]. This species increases in fraction with temperature, at the expenses of the Gaussian component [see Fig. 5(d)] In order to study the ion dynamics, we performed transverse field experiments at various temperatures and we fitted the data according to a simplified function

$$P_\mu(t) = A\cos(\gamma_\mu B_{ext} t + \phi)\exp(-\lambda_{TF} t) \quad (3)$$

Here A is the diamagnetic fraction (interstitial μ^+ and Mu-Li), γ_μ is the muon gyromagnetic ratio, B_{ext}=20 G, and λ_{TF} the transverse relaxation rate. Although the fit to Eq.3 would be correct for x=6, where a single Lorentzian decay reproduces the data; for x=0-3 two different decays would have been more appropriate to discern between the interstitial μ^+ and the Mu-Li species. However, the correlations between two different relaxations increase the inaccuracy and a single Lorentzian decay (rather than Gaussian) proves to be the best compromise to detect any changes in dynamics. The result of the fit [see Fig. 5(b)] highlights a transition that can be ascribed to the activation of Li dynamics experienced by interstitial muons. The assignment of this relaxation to interstitial muons is also supported by the similar trend of σ_{ZF}(T) found in the ZF experiment [Fig. 5(c)]. It is worthwhile to note that muons can also diffuse and the TF relaxation might include a concerted contribution of interstitial muons and Li ions. The TF data were fitted according to a two-state law that considers the contribution from excited and non-excited ions (Hendrickson *et al.*[25]). Values for the activation energies are reported in Table II. The activation energies calculated from the fits are an order of magnitude lower than that expected from the hopping of Li and Na (*i.e.* intersite diffusion) but they are in agreement with the values expected from an intra-site dynamics (*i.e.* diffusion of ions confined within the cluster), as found by means of NMR in $Na_xLi_{6-x}C_{60}$ compounds[26]. In $Li_{12}C_{60}$, previous investigations by means of inelastic neutron scattering also highlighted the intra-site dynamics of Li below room temperature[21]. It is therefore reasonable to assign these energies to the activation of intra site diffusion for Li. Low Na doping (x=1, 2) reflect into an increase of

TABLE II. Activation energies obtained from the fit of the transversal field relaxations for selected $Na_xLi_{12-x}C_{60}$ samples according to the two-state model of ref.[25].

x	E (kJ/mol)
0	5.4(5)
1	7.6(4)
2	8.7(3)
6	4.2(3)

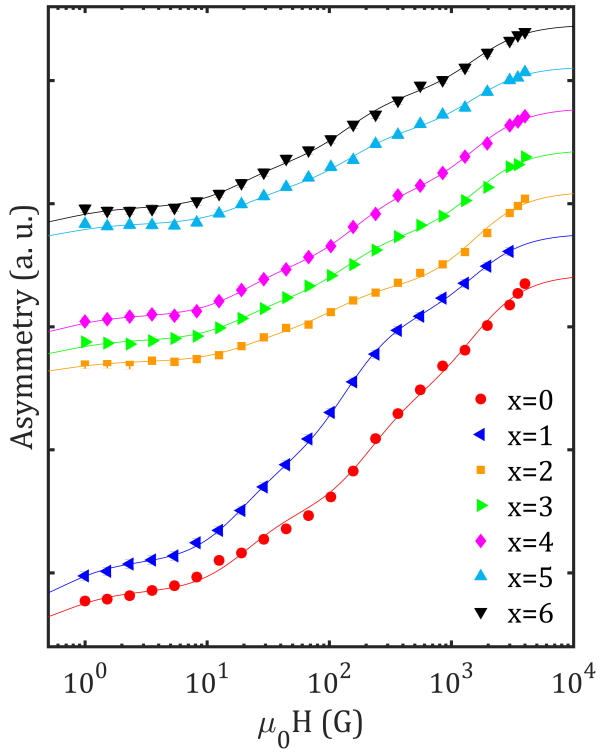

FIG. 6. LF repolarization of $Na_xLi_{6-x}C_{60}$ at T=5 K and fit according to Eq.4.

the energy barrier required for the activation of these motions, while for x=6 the effect is opposite. These results suggest that low doping levels of Na have a stabilizing effect on the Li dynamics. Concerning the interaction with hydrogen, the formation of Mu-Li species suggests that, during the triggering of the absorption, hydrogen atoms are more likely to be chemisorbed on Li clusters, rather than fullerene, leading to the facile formation of LiH.

$Na_xLi_{6-x}C_{60}$ compounds (y=6) For the $Na_xLi_{6-x}C_{60}$ series (*i.e.* y=6), the ZF μSR data do not show any particular feature other than a simple Lorentzian decay, ascribed to the dynamic interaction of μ^+ with ^{23}Na and ^{7}Li spins (see Fig. SI2). On the other hand, each sample displays a considerably lower initial asymmetry with respect to that expected (22.84%), suggesting the formation of muonium. In order to provide better insight on paramagnetic species, we carried out a series of LF experiments at low temperature (T=5 K) in order to freeze the rotation of fullerene. Fig. 6 shows the repolarization curves in $Na_xLi_{6-x}C_{60}$ (x=0-6) in the range 0-4 kG at 5 K. The data display multiple regimes that confirm the presence of anisotropic muonium radical adduct. Moreover, the polarization is not fully recovered at the highest field investigated, also suggesting the formation of endohedral muonium. Therefore, data have been fitted to a model considering the sum of three contributions:

$$P_\mu(t_0) = P_{\mu^+}(0) + P_{Mu}(A_i^{Mu}; B) + P_r(A_i^r, D_1, D_2; B) \quad (4)$$

Where P_{μ^+}, P_{Mu} and P_r, correspond to the fraction of diamagnetic muons (μ^+), endohedral muonium (Mu@C_{60}), and radical (Mu-C_{60}), respectively. A_i^{Mu} and A_i^r are the hyperfine frequencies relative to the endohedral and radical species respectively. D_1 and D_2 are the anisotropy parameters for the radical. D_2 and A_i^{Mu} were kept constant to those of pristine C_{60} (2.4 MHz and 4.3 GHz respectively) since we do not expect any particular variation of their values. The results of the fit are reported in Table III. Compared to pure C_{60}, where the adduct radical has A_i^r=325 MHz and D_1=10.67 MHz[27], $Na_xLi_{6-x}C_{60}$ compounds display higher values of A_i^r and D_1. This might indicate a more efficient localization of the radical electron and a larger anisotropy of the hyperfine interaction, respectively. Moreover, the electronic configuration in alkali-intercalated fullerides is different as a consequence of the substantial charge transfer on C_{60}. This charged state is likely to affect the delocalization of the radical electron with respect to the neutral state. On the other hand, the reduced symmetry induced by the intercalation of alkali metals, the static disorder of C_{60}, and the disordered occupancy of Li and Na sites in the fulleride lattice can affect the local structure of the radical, leading to a distribution of the hyperfine parameters, therefore the fitted values of A_i^r and D_1 can be considered as average values. As expected, the fraction of endohedral muonium is almost independent of Na content. On the contrary, the formation of radicals is highly promoted for the y=6 family, especially for samples with low concentration of Na, reaching a maximum for x=1, which is in agreement with the recently reported H_2 sorption performance of this sample[10].

TABLE III. Radical and endohedral muonium fractions (the remaining fraction is given by diamagnetic muons), radical hyperfine, and D_1 as function of x for $Na_xLi_{6-x}C_{60}$.

x	Mu-C_{60} (%)	Mu@C_{60} (MHz)	A_i^{rad} (MHz)	D_1 (MHz)
0	46(2)	45(2)	596(43)	60(7)
1	53(2)	29(2)	390(22)	54(4)
2	15(1)	32(1)	315(38)	61(9)
3	23(1)	30(1)	396(51)	57(9)
4	29(1)	31(2)	456(49)	59(8)
5	22(1)	24(1)	424(63)	60(10)
6	26(1)	26(1)	400(50)	53(8)

IV. CONCLUSIONS

Mixed Na and Li $Na_xLi_{y-x}C_{60}$ fullerides (y=6 and 12) were synthesized by means of a two-step mechanochemical procedure. The structural and spectroscopic properties of $Na_xLi_{12-x}C_{60}$ were investigated by means of

XRPD and Raman spectroscopy. Diffraction data highlighted an increase of the *fcc* lattice constant with x, although the lattice volume is contracted compared to the Na_6C_{60} parent structure, due to the strong electrostatic interaction between charged fullerenes and Li ions. The charge transfer from the intercalated metals to C_{60} was evaluated by means of Raman spectroscopy. We found that 5-7 electrons (depending on x) are transferred to the anti-bonding orbitals of fullerene. Besides, Li, rather than Na, seems to be more effective in donating its charge to C_{60}, possibly reducing the icosahedral symmetry of the molecule. PCT-DSC measurements highlighted good and reversible sorption performance up to x=3 concerning gravimetric capacity and absorption kinetics, but the onset temperature for desorption and the desorption enthalpies are lower and more promising for higher Na content. In general, the y=6 family showed better sorption performance with respect to y=12. This behaviour was explored by means of muon spectroscopy. We observed that for y=6, muonium radical adducts are easily formed on the external surface of fullerene and their fraction reaches a maximum for x=1 with an efficient delocalization of the radical electron. This species is chemically equivalent to the formation of a C-H bond on fullerene. For y=12, muonium preferentially binds to Li in a covalent manner. This species might be considered as the prototype of LiH, which is segregated during the H_2 absorption process, negatively effecting the H_2 sorption performance.

ACKNOWLEDGMENTS

This work has received support from the European Union's Horizon 2020 research and innovation programme under the Marie Sklodowska-Curie Grant Agreement 665593 awarded to the Science and Technology Facilities Council. We would like to thank Dr. Gavin Stenning for the help with the XRD measurement.

[1] K. R. S. Chandrakumar and S. K. Ghosh, Nano letters **8**, 13 (2008), ISSN 1530-6984, URL http://www.ncbi.nlm.nih.gov/pubmed/18085807.

[2] Q. Sun, P. Jena, Q. Wang, and M. Marquez, Journal of the American Chemical Society **128**, 9741 (2006), ISSN 0002-7863, URL http://www.ncbi.nlm.nih.gov/pubmed/23160931http://www.ncbi.nlm.nih.gov/pubmed/16866529.

[3] J. A. Teprovich, M. S. Wellons, R. Lascola, S.-J. Hwang, P. a. Ward, R. N. Compton, and R. Zidan, Nano letters **12**, 582 (2012), ISSN 1530-6992, URL http://www.ncbi.nlm.nih.gov/pubmed/22206302.

[4] P. Mauron, A. Remhof, A. Bliersbach, A. Borgschulte, A. Züttel, D. Sheptyakov, M. Gaboardi, M. Choucair, D. Pontiroli, M. Aramini, et al., International Journal of Hydrogen Energy **37**, 14307 (2012), ISSN 03603199, URL http://linkinghub.elsevier.com/retrieve/pii/S0360319912016229.

[5] A. Yoshida, T. Okuyama, T. Terada, and S. Naito, Journal of Materials Chemistry **21**, 9480 (2011), ISSN 0959-9428, URL http://xlink.rsc.org/?DOI=c1jm11542ahttp://www.rsc.org/suppdata/jm/c1/c1jm11542a/c1jm11542a.pdf.

[6] T. Yildirim, O. Zhou, J. E. Fischer, N. Bykovetz, R. A. Strongin, M. A. Cichy, A. B. Smith III, C. L. Lin, and R. Jelinek, Nature **360**, 568 (1992), ISSN 0028-0836, URL http://www.nature.com/doifinder/10.1038/360568a0.

[7] F. Giglio, D. Pontiroli, M. Gaboardi, M. Aramini, C. Cavallari, M. Brunelli, P. Galinetto, C. Milanese, and M. Riccò, Chemical Physics Letters **609**, 155 (2014), ISSN 00092614, URL http://linkinghub.elsevier.com/retrieve/pii/S0009261414005417.

[8] P. Mauron, M. Gaboardi, D. Pontiroli, A. Remhof, M. Riccò, and A. Züttel, The Journal of Physical Chemistry C **119**, 1714 (2015), ISSN 1932-7447, URL http://pubs.acs.org/doi/abs/10.1021/jp511102y.

[9] N. Sarzi Amadè, M. Gaboardi, G. Magnani, M. Riccò, D. Pontiroli, C. Milanese, A. Girella, P. Carretta, and S. Sanna, International Journal of Hydrogen Energy **42**, 22544 (2017), ISSN 03603199, URL http://linkinghub.elsevier.com/retrieve/pii/S0360319917307644.

[10] M. Gaboardi, C. Milanese, G. Magnani, A. Girella, D. Pontiroli, P. Cofrancesco, A. Marini, and M. Ricco, Phys. Chem. Chem. Phys. pp. 21980–21986 (2017), ISSN 1463-9076, URL http://pubs.rsc.org/en/Content/ArticleLanding/2017/CP/C7CP04353H.

[11] F. Pratt, Physica B: Condensed Matter **289-290**, 710 (2000), ISSN 09214526, URL http://linkinghub.elsevier.com/retrieve/pii/S0921452600003288.

[12] N. Sarzi Amadè, D. Pontiroli, L. Maidich, M. Ricco, M. Gaboardi, G. Magnani, P. Carretta, and S. Sanna, The Journal of Physical Chemistry C **121**, acs.jpcc.7b00887 (2017), ISSN 1932-7447, URL http://pubs.acs.org/doi/abs/10.1021/acs.jpcc.7b00887.

[13] M. J. Rosseinsky, D. W. Murphy, R. M. Fleming, R. Tycko, A. P. Ramirez, G. Dabbagh, and S. E. Barrett, Nature **356**, 416 (1992), ISSN 0028-0836, URL http://www.nature.com/doifinder/10.1038/356416a0.

[14] P. Dresselhaus, M.S., Dresselhaus, G., Eklund, Journal of Physical Chemistry **27**, 351 (1996), ISSN 03770486.

[15] T. Wågberg, P. Stenmark, and B. Sundqvist, Journal of Physics and Chemistry of Solids **65**, 317 (2004), ISSN 00223697, URL http://linkinghub.elsevier.com/retrieve/pii/S0022369703004128.

[16] S. J. Blundell, Contemporary Physics **40**, 175 (1999), ISSN 0010-7514, 0207699, URL http://arxiv.org/abs/cond-mat/0207699http://www.tandfonline.com/doi/abs/10.1080/001075199181521.

[17] W. MacFarlane, R. Kiefl, S. Dunsiger, J. Sonier, J. Chakhalian, J. Fischer, T. Yildirim, and K. Chow, Physical Review B **58**, 1004 (1998), ISSN 0163-1829, URL http://link.aps.org/doi/10.1103/PhysRevB.58.1004.

[18] R. Kiefl, T. Duty, J. Schneider, A. MacFarlane, K. Chow, J. Elzey, P. Mendels, G. Morris, J. Brewer, E. Ansaldo, et al., Physical Review Letters **69**, 2005 (1992), ISSN 0031-9007, URL http://link.aps.org/doi/

10.1103/PhysRevLett.69.2005.

[19] M. Aramini, M. Gaboardi, G. Vlahopoulou, D. Pontiroli, C. Cavallari, C. Milanese, and M. Riccò, Carbon **67**, 92 (2014), ISSN 00086223, URL http://linkinghub.elsevier.com/retrieve/pii/S0008622313009172.

[20] M. Gaboardi, N. Sarzi Amadé, M. Aramini, C. Milanese, G. Magnani, S. Sanna, M. Riccò, and D. Pontiroli, Carbon **120**, 77 (2017), ISSN 00086223, URL http://linkinghub.elsevier.com/retrieve/pii/S0008622317304712.

[21] M. Gaboardi, C. Cavallari, G. Magnani, D. Pontiroli, S. Rols, and M. Riccò, Carbon **90**, 130 (2015), ISSN 00086223, URL http://www.sciencedirect.com/science/article/pii/S0008622315002808http://linkinghub.elsevier.com/retrieve/pii/S0008622315002808.

[22] P. F. Meier, Hyperfine Interactions **18**, 427 (1984), ISSN 0304-3834, URL http://link.springer.com/10.1007/BF02064848.

[23] M. Celio and P. F. Meier, Hyperfine Interactions **18**, 435 (1984), ISSN 0304-3834, URL http://link.springer.com/10.1007/BF02064849.

[24] G. Herzberg, *Molecular Spectra and Molecular Structure I. Spectra of Diatomic Molecules, 2nd ed.* (Van Nostrand, 1950).

[25] J. R. Hendrickson and P. J. Bray, Journal of Magnetic Resonance (1969) **9**, 341 (1973), ISSN 00222364.

[26] N. Sarzi Amadè, D. Pontiroli, L. Maidich, M. Ricco, M. Gaboardi, G. Magnani, P. Carretta, S. Sanna, M. Riccò, M. Gaboardi, et al., The Journal of Physical Chemistry C **121**, 6554 (2017), ISSN 1932-7447, URL http://pubs.acs.org/doi/abs/10.1021/acs.jpcc.7b00887.

[27] R. Macrae, R. Kadono, F. Pratt, and K. Tanigaki, Hyperfine Interactions **106**, 175 (1996), ISSN 1572-9540, URL http://www.springerlink.com/index/H42H7384456V3744.pdf{%}5Cnpapers://9bb24574-0455-468e-81e7-d359f00c1207/Paper/p204.